Electronic supplementary information (ESI)

Improving the Capacity and Cycling-Stability of Lithium−Sulfur Batteries by Self-Healing Binders Containing Dynamic Disulfide Bonds

Lei Duan [a,1], Weihua Kong[a,1], Wen Yan[a], Cheng-Hui Li[a,*], Zhong Jin[a,*], Jing-Lin Zuo[a,*]

[a] State Key Laboratory of Coordination Chemistry, Key Laboratory of Mesoscopic Chemistry of MOE, Jiangsu Key Laboratory of Advanced Organic Materials, School of Chemistry and Chemical Engineering, Collaborative Innovation Center of Advanced Microstructures, Nanjing University, Nanjing 210093, P. R. China

[1]These authors contributed equally to this work.

*Corresponding author.
E-mail: chli@nju.edu.cn (Cheng-Hui Li); zhongjin@nju.edu.cn (Zhong Jin); zuojl@nju.edu.cn (Jing-Lin Zuo)

Experimental Section

Materials and general measurements. Poly(dimethylsiloxane) bis(3-am inopropyl) terminated (H_2N-PDMS-NH_2, M_n = 700-900) was purchased from Gelest. All chemicals were purchased from commercial sources and used without further purification. Scanning electronic microscopy (SEM) images and energy dispersive X-ray spectroscopy (EDX) profiles were taken on Japan Hitachi S-4800 field emission SEM and FEI NanoSEM Nova-450 equipped with Bruker Quantax-200. X-ray photoelectron spectroscopy (XPS) were obtained using a Thermo ESCALAB 250 X-ray photoelectron spectrometer with Al K_α radiation. Differential Scanning Calorimetry (DSC) experiments were performed using a Mettler-Toledo DSC1 STARe differential scanning calorimeter. The temperature range was -90 °C to 50 °C at a heating and cooling speed of 10 °C/min under a nitrogen atmosphere. Thermogravimetric analyses were measured with a SDT 2960 thermal analyzer from 30 to 800 °C at a heating rate of 10 °C/min under N_2 atmosphere. ^{1}H NMR (400 MHz) spectra were recorded on a Bruker DRX 400 NMR spectrometer in deuterated solvents at room temperature (25 °C). FTIR spectra were performed on a Bruker Tensor27 FTIR spectrophotometer. Relative molecular weights of binder were carried out on a Malvern VE2001 gel permeation chromatography (GPC). The rheological behaviors were carried out on a TA Instruments DHR-2 system. Dynamic oscillatory strain sweeps were measured at f = 1 Hz. Frequency sweep measurements with 1% strain amplitude were run from 0.06 to 1000 rad/s at 25 °C.

Synthesis of 2S-PDMS-9/1 polymer. Et_3N (3.5 mL), 4-Aminophenyl disulfide (248.4 mg, 1 mmol, defined as 2S) and H_2N-PDMS-NH_2 (6.3 g, 9 mmol) were together dissolved in anhydrous CH_2Cl_2 (80 mL) and vigorously stirred at 0 °C for 1 h. 2,6-pyridinedicarbonyl dichloride (2.04 g, 10 mmol) was added to anhydrous CH_2Cl_2 (20 mL) and slowly dropped into the mixed solution under argon atmosphere. After reaction for 24 hours, the mixed solution was concentrated to about 2 mL and 40 mL MeOH was poured into it to dissolve Et_3N in reaction. Yellow precipitate-like viscous liquid appeared and the mixture was settled for 30 min. The upper clear solution was then removed. After repeated for three times, the concentrated solution was poured into a polytetrafluoroethene (PTFE) mold and dried at 80 °C for 12 h. Molecular

weight according to GPC: M_w = 21,090; M_n = 9,390 ($Đ$ = 2.245). ^{1}H NMR (400 MHz, $CDCl_3$): δ(ppm) 8.37, 8.30, 8.28, 8.03, 7.95, 7.66, 7.19, 3.42, 1.61, 0.54.

2S-PDMS were synthesized using different mixing molar ratio of 2S and H_2N-PDMS-NH_2 according to the same procedure as that used for 2S-PDMS-9/1. For 2S-PDMS-x/y, mixture of H_2N-PDMS-NH_2 (x eq) and 2S (y eq) was used. The H_2N-PDMS-NH_2 to 2S molar ratio for the 2S-PDMS-x/y polymer is respectively 1: 0, 7: 3, 8: 2, 9: 1 and 10: 1, corresponding to the PDMS, 2S-PDMS-7/3, 2S-PDMS-8/2, 2S-PDMS-9/1(2S-PDMS, generally for short, No special circumstances) and 2S-PDMS-10/1.

Preparation of sulfur/carbon (S/C) composite materials. 600 mg sulfur powders and 400 mg porous carbon (Ketjenblack EC600JD, KJC) with ratio of 3: 2 were ground homogeneously and were heated at 155 °C for 16 h. The sulfur content of the composite materials is to 60 wt.%, as determined by TGA (Fig. S14). Sulfur/carbon composite materials with a sulfur content of 70 wt.% and 80 wt.% were prepared according to the same procedure as that used.

Preparation of 2S-PDMS-S electrode. The 2S-PDMS-S electrode was prepared by mixing 80 wt.% of sulfur/carbon composite materials (generally used a sulfur content of 60 wt.%, No special circumstances), 10 wt.% of acetylene black, and 10 wt.% of 2S-PDMS polymer binder in N-methyl-2-pyrrolidone (NMP) solvent. For electrodes used for soft-packed batteries, the sulfur content in S/C is 80%. For electrodes used for SEM observation, the slurry was prepared by mixing pure sulfur (80 wt.%) with 10 wt.% AB and 10 wt.% binders. The slurry was then applied uniformly on a carbon coated aluminum foil by a doctor blade. The asprepared electrode was finally obtained after drying in a vacuum oven at 60 °C overnight and the overall sulfur loading was about 0.8-1.1 mg cm^{-2}.

The conductive composite was prepared by mixing 80 wt.% of 2S-PDMS polymer and 20 wt.% acetylene black (AB).

Preparation of PVDF-S Electrode. For comparison, sulfur electrodes with polyvinylidene fluoride (PVDF) binder were also prepared in the same processes.

Mechanical and self-healing tests. All stress-strain curves were obtained from an Instron 3343 instrument. Tested samples (60 mm length × 5 mm width × 1 mm height) were fixed on the jigs of the tension machine. The mechanical tensile-stress was measured at a strain rate of 10 mm min^{-1} with gauge length of 5 mm. For self-healing tests, the polymer film was cut into two identical pieces with a razor blade and then

contacted together. After healing at ambient temperatures for different time, the stress-strain curves of the healed polymer were obtained from the same procedure. The self-healing efficiency was calculated by the ratio of the maximal strength restored relative to the original maximal strength.

Adhesive tests. The polymer (1.0 g) was swelled in THF (5 mL) to obtain the low-viscosity glue. Each glue (50 mg) was smeared between the two substrates (100 mm × 20 mm × 2 mm) to form an overlapped structure. The overlapped area was fixed as 2.0 cm × 2.0 cm. The two substrates samples were dried at 80 °C for 6 h. The shear strength experiments were performed on an Instron 4200 Microtester at a strain rate of 50 mm/min.

Batteries assembly and electrochemical tests. The CR2032 type coin cells were assembled in an Argon-filled glovebox with oxygen and water content under 0.1 ppm. 1M lithium bis-(trifluoromethane) sulfonamide (LiTFSI) in a solution of 1,3-dioxolane (DOL) and dimethoxyethane (DME) with 1/1 volume ratio with 1% $LiNO_3$ as additive was selected as electrolyte. Commercial polypropylene-based porous membrane (Celgard 2400) was chosen as separator. The dosage of electrolyte was 20 μL per cells. Electrochemical impedance spectrums (EIS) and cyclic voltammetry (CV) tests were conducted on electrochemical workstation (RST5200F, Rui Sitai, Soochow). EIS was acquired from 1 MHz to 10 mHz with bias potential of 5 mV. CV curves were acquired within 1.7-2.6 V at scan rate of 0.1 mV s^{-1}. All galvanostatic cycling was performed on the Land CT2001 (LanHe, Wuhan) multichannel battery tester with voltage window of 1.7-2.6 V.

Li_2S_6 symmetric cells test. Li_2S_6 solution was prepared by adding 19.2 mg lithium sulfide and 66.7 mg high-purity sulfur into 1 mL dimethoxyethane to form a solution with 2.5 M [S], which was further stirred magnetically at 50 °C for 24 h in an Ar-filled glove-box. The mixture of 2S-PDMS or PVDF with equal-mass super P was prepared into a slurry in NMP and was then cast on carbon paper (CP), denoted as 2S-PDMS/CP and PVDF/CP. Two identical electrodes were assembled into a CR 2032 coin cell with Celgard 2400 separator, 40 μL Li_2S_6 solution added. CV curves were acquired at a scan rate of 3 mV s^{-1} between -1 V and 1 V.

Nucleation of lithium sulfide. Li_2S_8 solution was prepared by mixing 224 mg sulfur and 46 mg Li_2S in 1.6 mL tetraglyme followed by magnetic stirring at 50 °C over night, forming a solution with 5 M [S]. To obtain the final catholyte, extra 459 mg LiTFSI and 33 mg $LiNO_3$ were added into above solution. 2S-PDMS/CP and

PVDF/CP was assembled with lithium foil, commercial PP separator, 20 μL catholyte and 20 μL blank electrolyte (1 M LiTFSI and 0.3 M $LiNO_3$ in tetraglyme) in a standard CR 2032 coin cells. The batteries were discharged galvanostatically at 0.112 mA to 2.05 V and then kept potentiostatically at 2.04 V for Li_2S to nucleate and grow. As the current was below 0.01 mA, the procedure would cease.

Computational Details. DFT calculations at B3LYP[1]/6-31 g (d) [2-5] level were carried out to optimize the geometries of various molecules. Single point energy calculations were conducted at B2PLYP[6]/def2tzvp[7] level and use the ZPE (zero point energy) to revise the whole energy. Integral equation formalism variant of the Polarizable Continuum Model (IEFPCM) [8-12] with parameters of dielectric constant ε = 7.2 was used. The above calculations were carried out with Guassian 09 package.[13] Because the PDMS chain mainly acted as a crosslinking and flexible scaffold, the reacting sites with polysulfides in 2S-PDMS molecules were almost from the parts of N^2, $N^{2'}$-(disulfanediylbis(4, 1-phenylene)) bis(pyridine-2, 6-dicarboxamide), denoted as DPPD next.

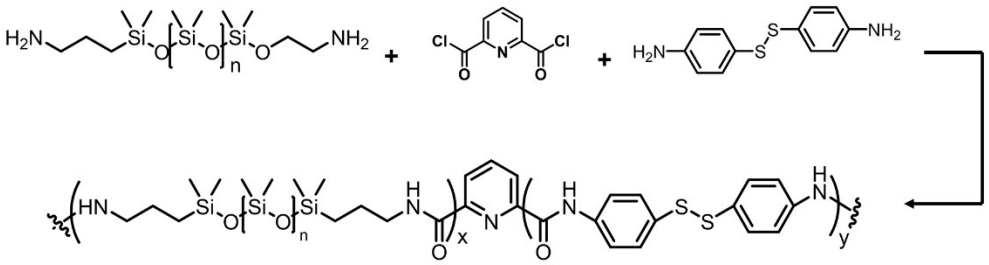

Fig. S1. Synthesis and chemical structure of the self-healing 2S-PDMS.

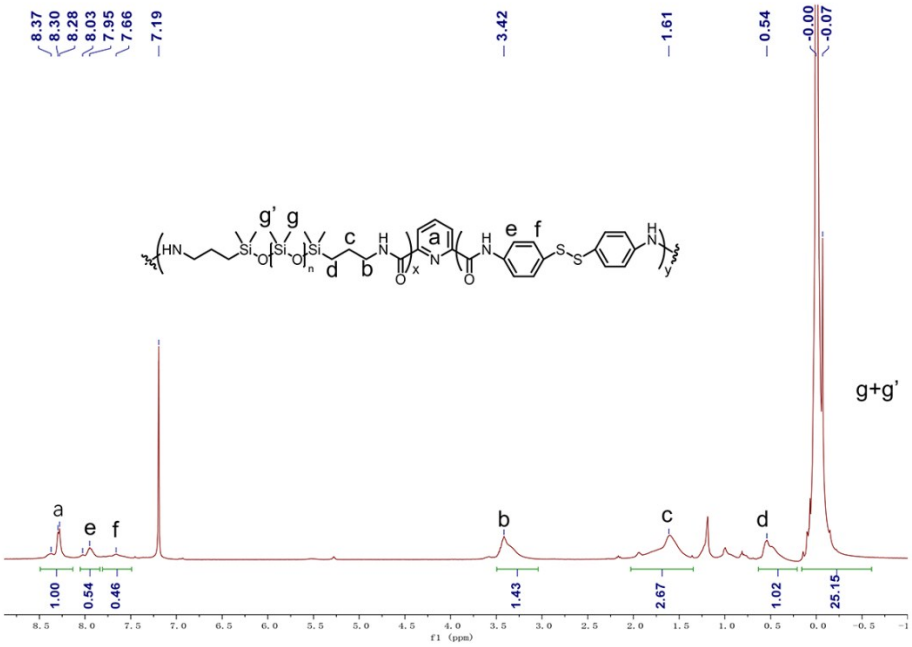

Fig. S2. ^{1}H NMR and spectra of 2S-PDMS polymer.

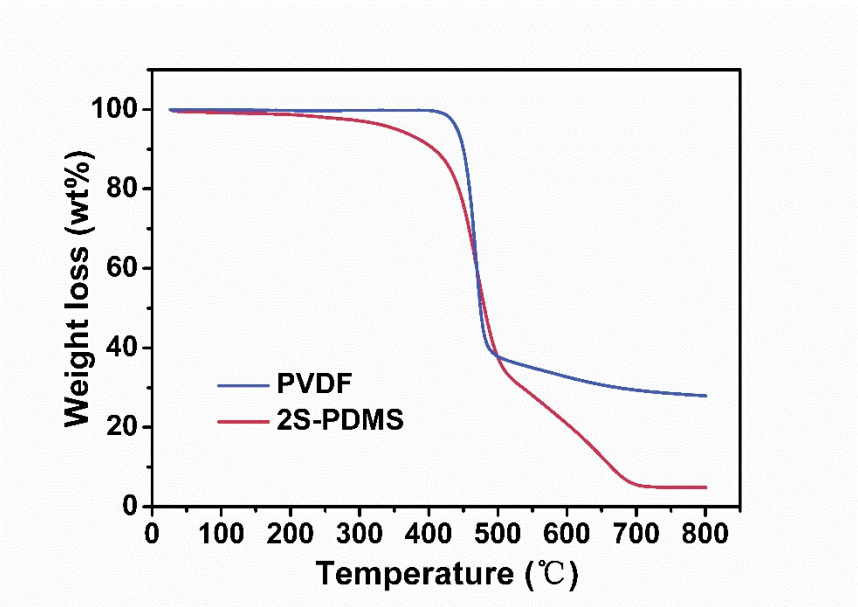

Fig. S3. The TGA curves of PVDF and 2S-PDMS polymer from room temperature to 800 °C under N_2 atmosphere.

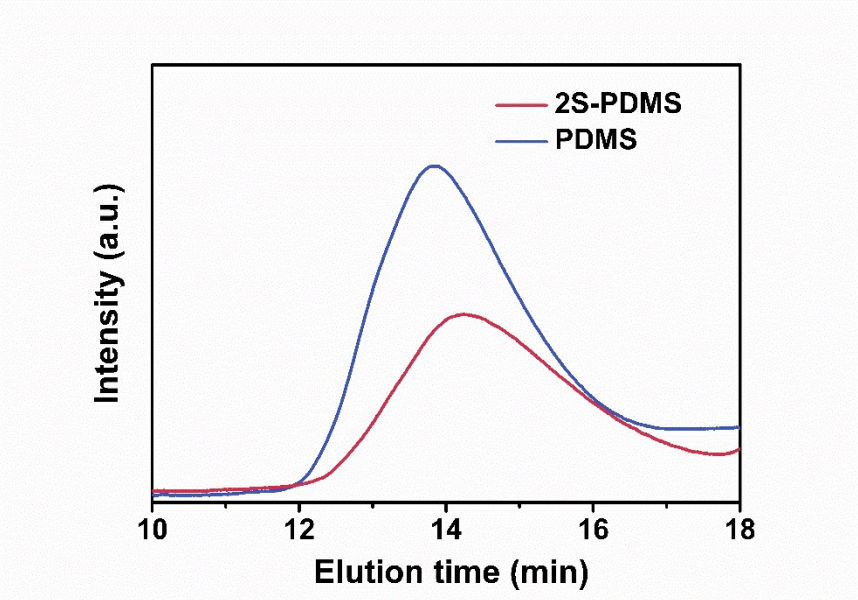

Fig. S4. GPC elution curves of PDMS and 2S-PDMS. Molecular weight of PDMS according to GPC: M_w = 28,810; M_n = 14,230 ($Đ$ = 2.025). Molecular weight of 2S-PDMS according to GPC: M_w = 21,090; M_n = 9,390 ($Đ$ = 2.245).

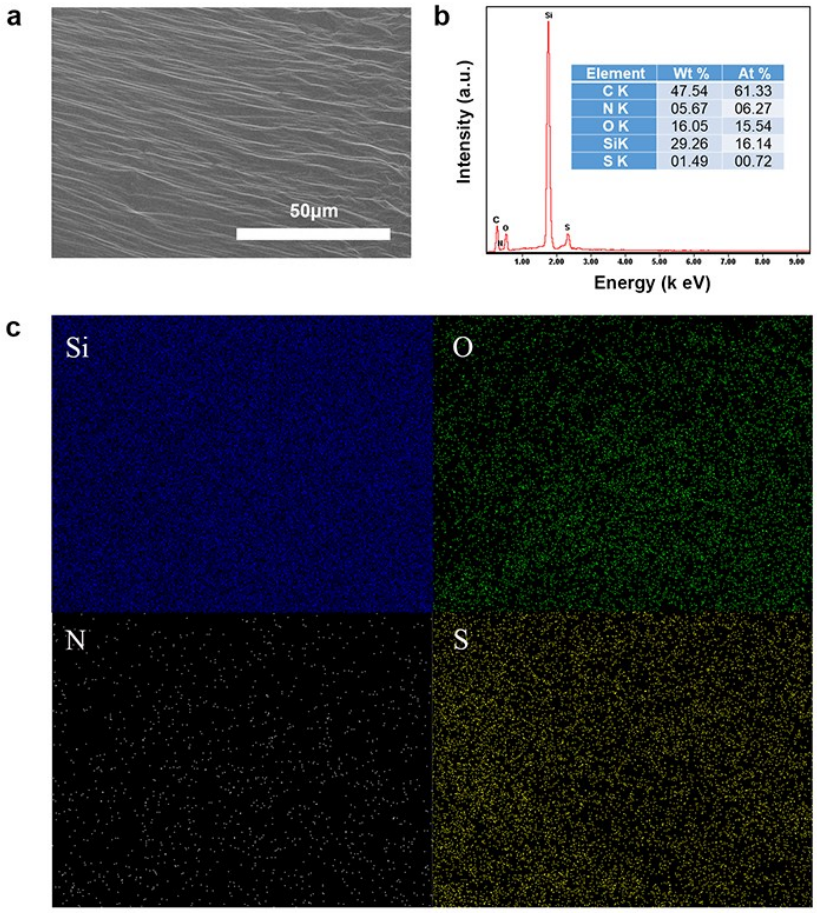

Fig. S5. SEM image (a) and EDX spectra (b) of 2S-PDMS polymer. Elemental mapping (c) of the 2S-PDMS.

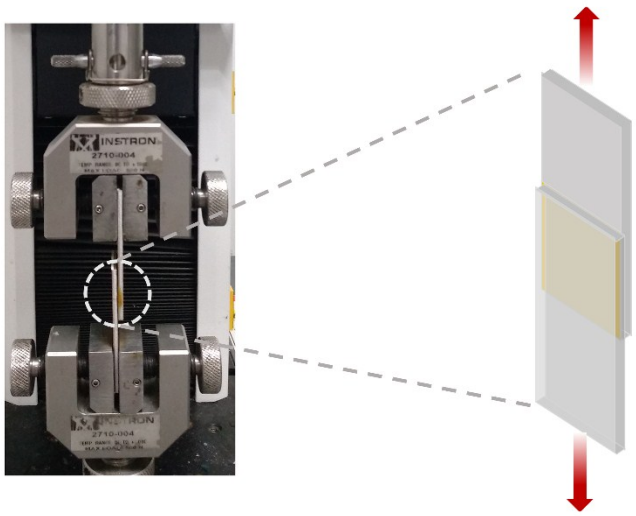

Fig. S6. Optical image of the setup, and schematic of the sample for the adhesive test.

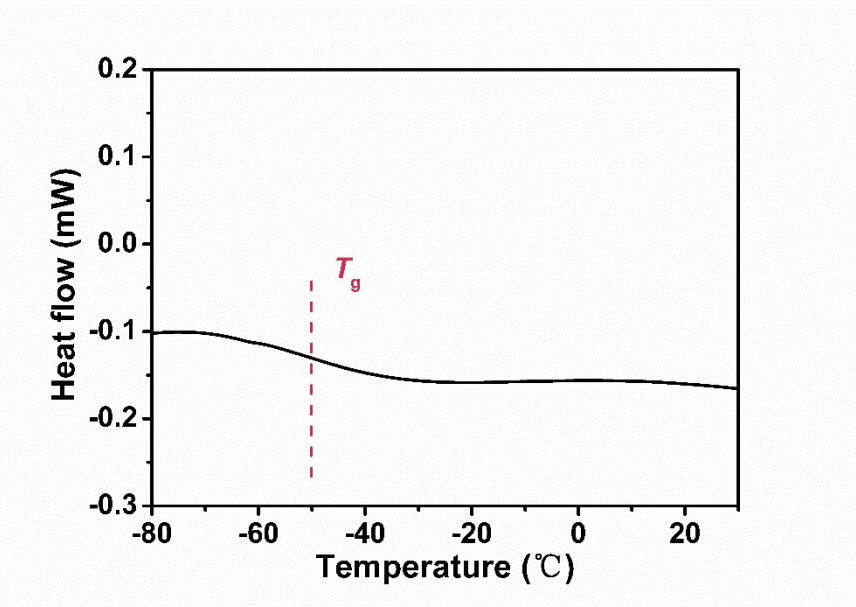

Fig. S7. The DSC curve of 2S-PDMS polymer.

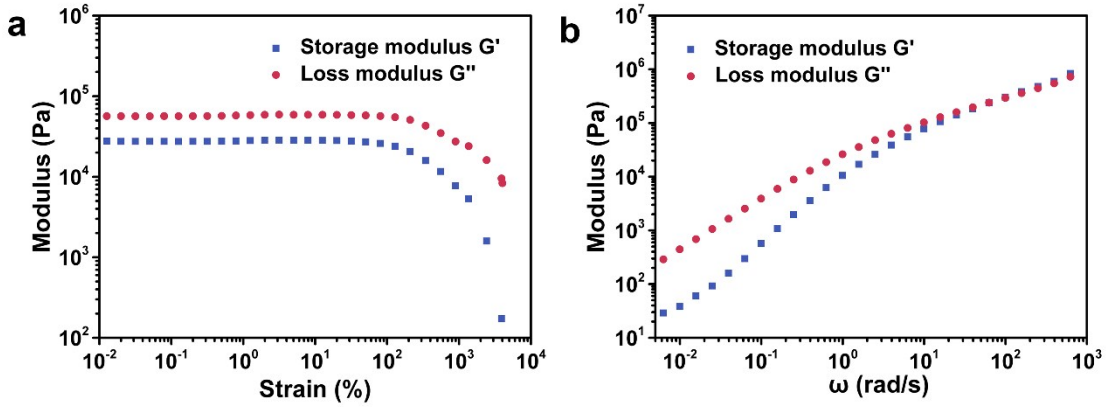

Fig. S8. Dynamic oscillatory strain sweep (a) and frequency sweep measurement (b) of 2S-PDMS polymer at 25 °C.

According to the strain sweep curve, the storage modulus G' is lower than the loss modulus G" at room temperature, indicating the material exhibits viscous-like behavior, dissipating more energy than it can store. As shown in Supplementary Fig. 8b, an intersection point between G' and G" at 10^2 rad/s shows the characteristic relaxation time of the polymer calculated was only 0.01 s at 25 °C. The rheological properties also suggest the good dynamic property of 2S-PDMS.

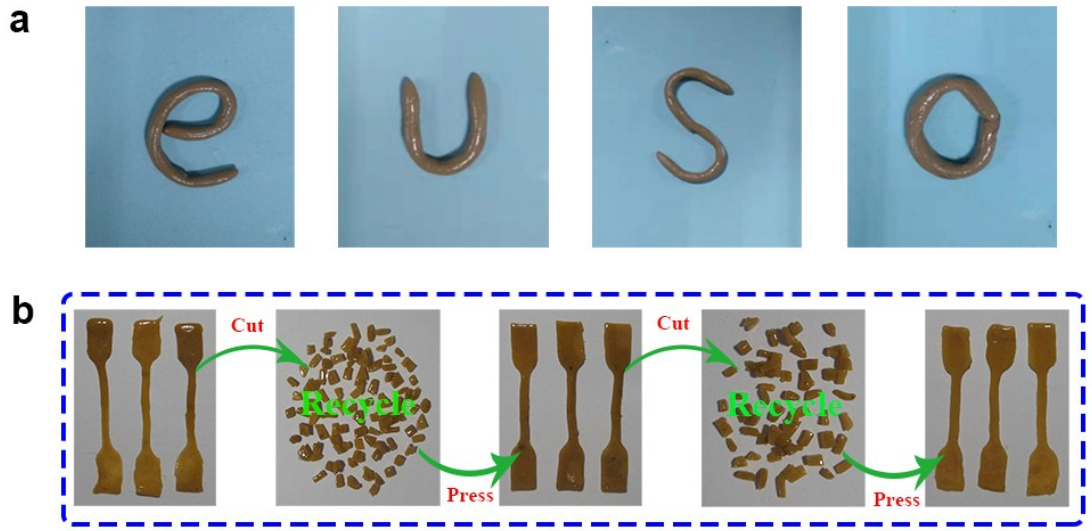

Fig. S9. Digital photos (a) of the 2S-PDMS showed good flexibility. (b)Typical recycling of 2S-PDMS polymer through compression molding at room temperature and 1 MPa for 10 min.

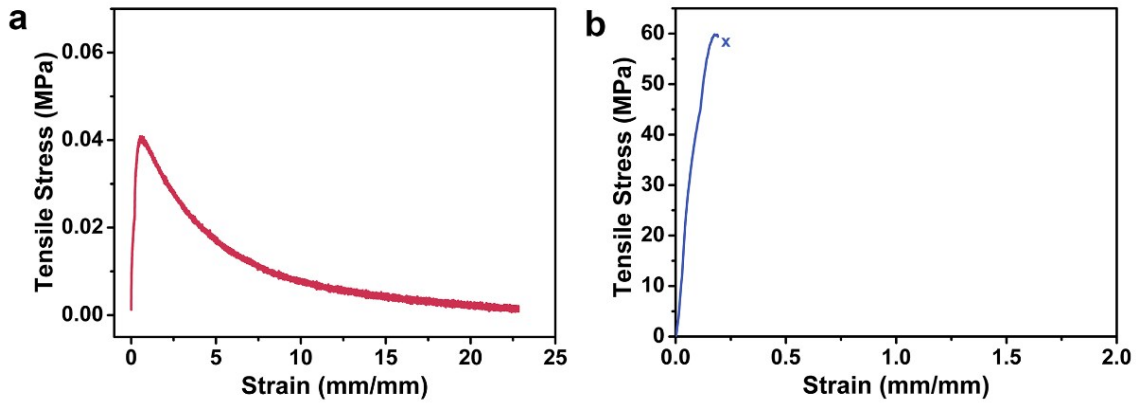

Fig. S10. The stress-strain curve of the 2S-PDMS polymer (a) and PVDF film (b) at room temperature.

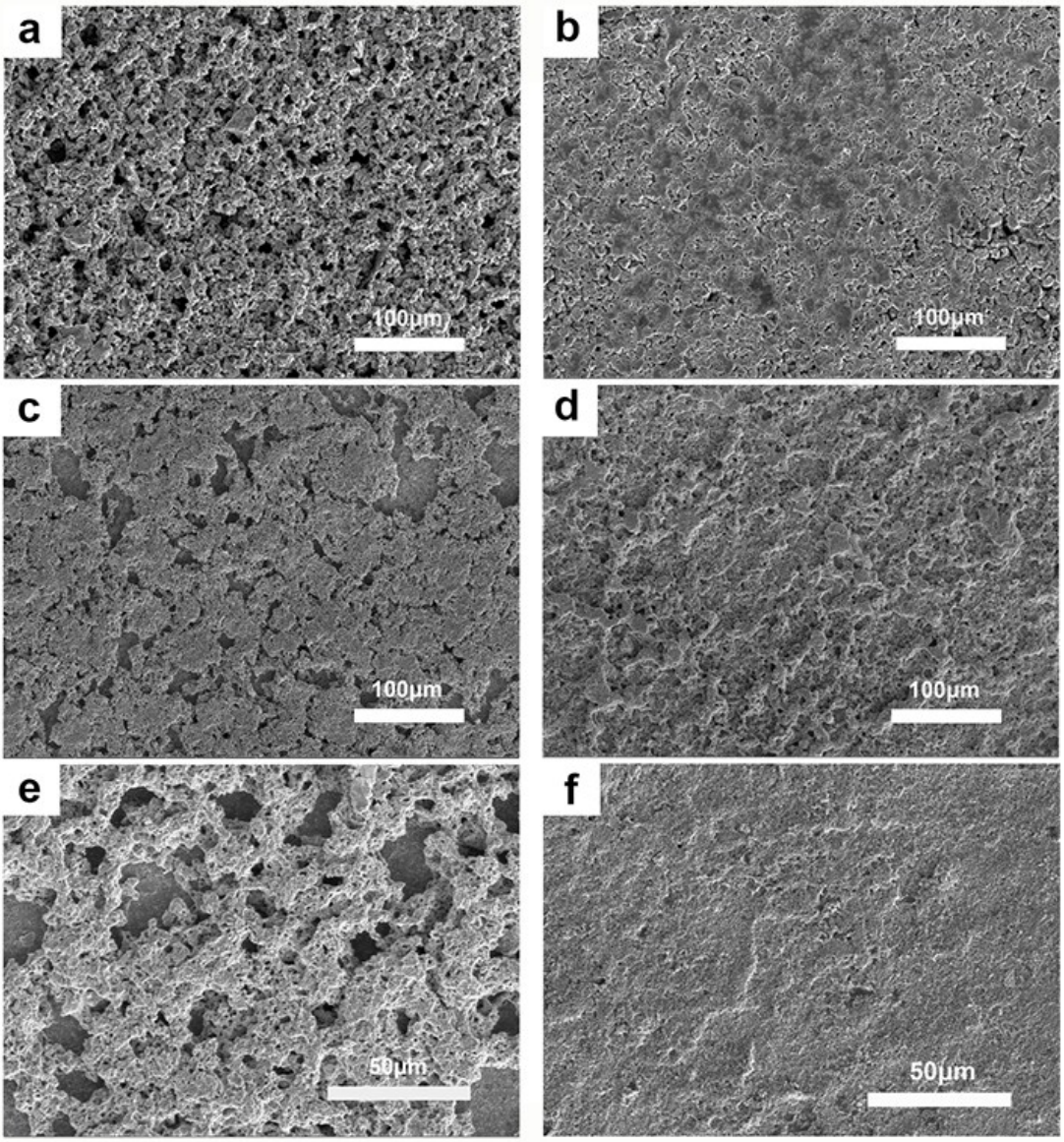

Fig. S11. SEM images of sulfur cathodes with PVDF polymer (a) and 2S-PDMS polymer binders (b) before cycling, respectively. SEM images of sulfur cathodes with PVDF polymer (c) and 2S-PDMS polymer binders (d) after 5 cycles at a rate of C/10, respectively. The origin SEM images (e) and (f) corresponding to Fig. 2 (c) and (d), respectively.

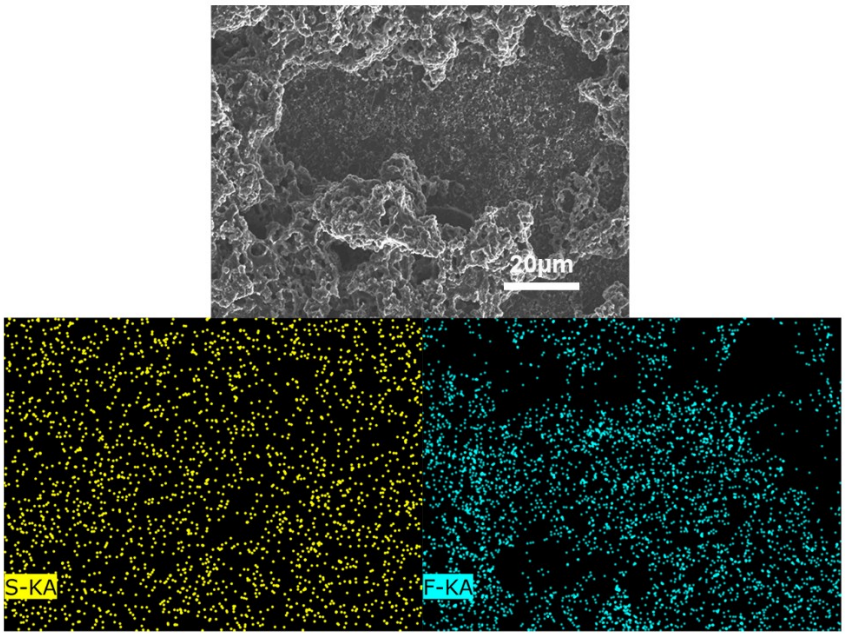

Fig. S12. SEM image and elemental mapping (S, and F elements) of PVDF-S electrode after cycling.

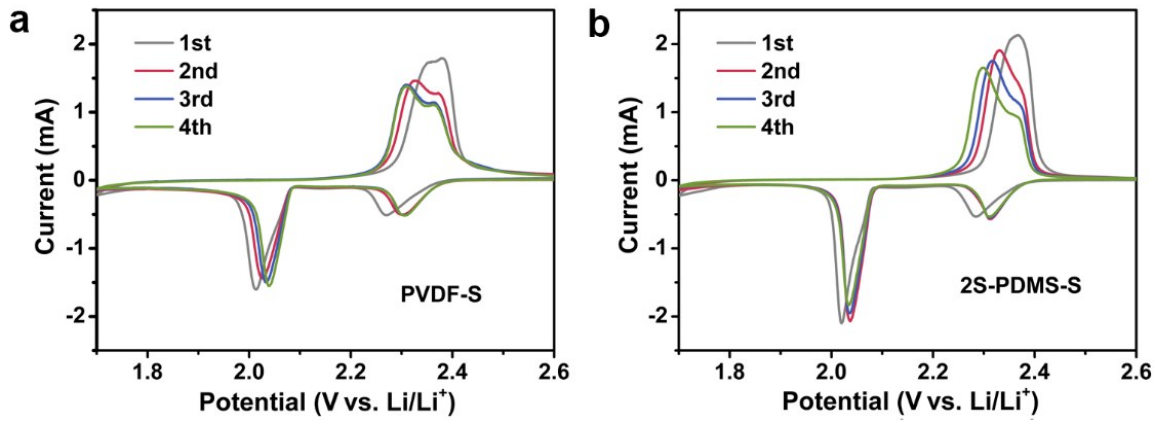

Fig. S13. CV curves of the first four scan for PVDF-S electrode (a) and 2S-PDMS-S electrode (b) at a scan rate of 0.1 mVs^{-1}.

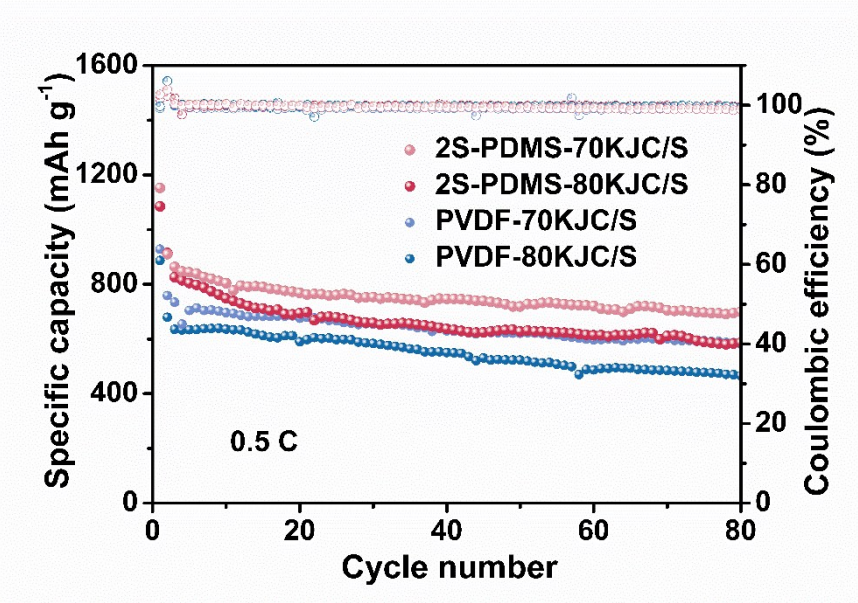

Fig. S14. Cycling performance of PVDF-S and 2S-PDMS-S with different sulfur content of KJC/S active material at 0.5 C.

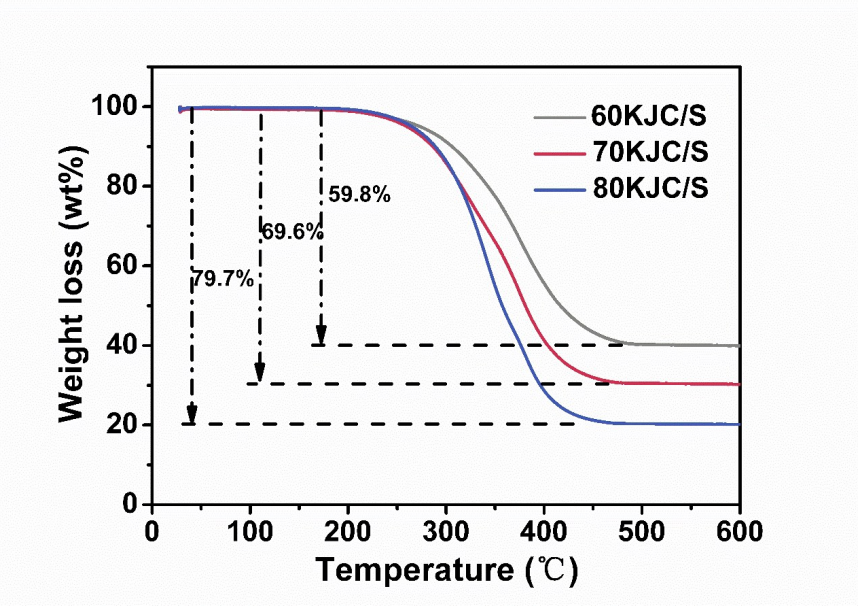

Fig. S15. The TGA curves of 60KJC/S, 70KJC/S and 80KJC/S composites from room temperature to 600 °C under N_2 atmosphere.

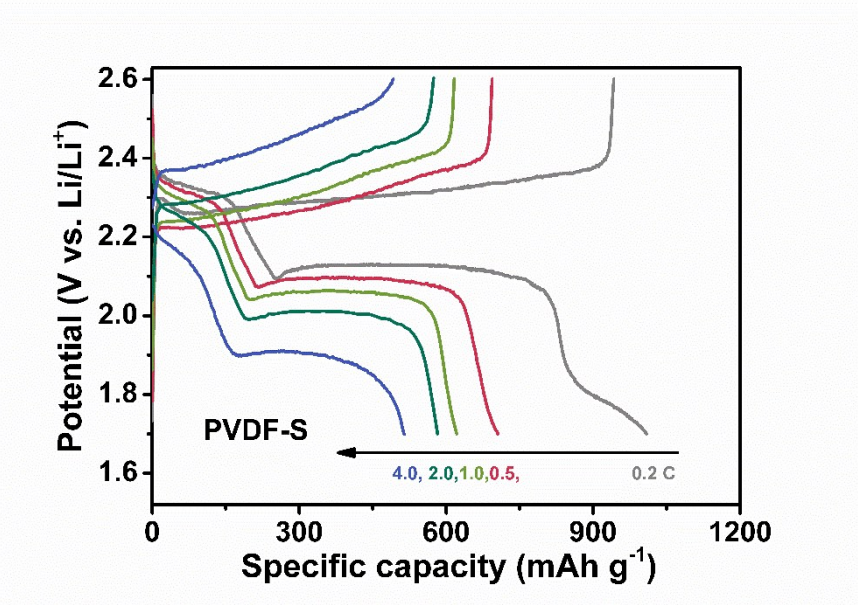

Fig. S16. Galvanostatic charge-discharge profiles of PVDF-S electrode at various current rates.

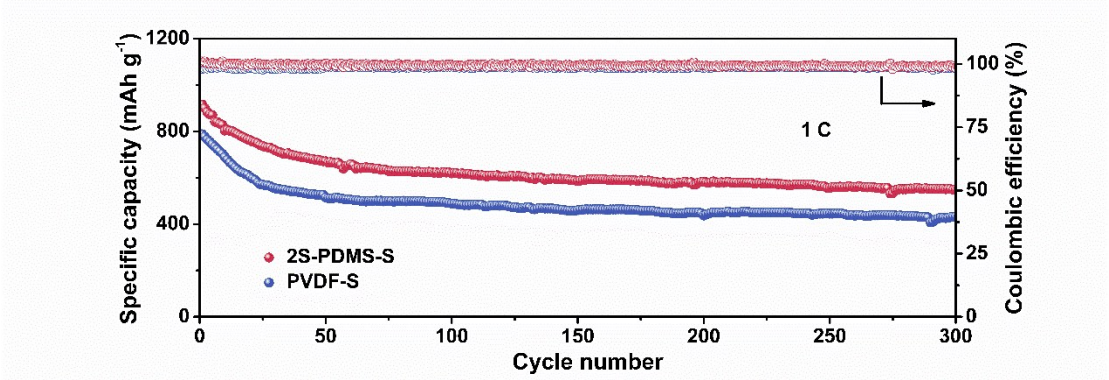

Fig. S17. Cycling performance of sulfur electrodes with PVDF and 2S-PDMS polymer binder at 1 C.

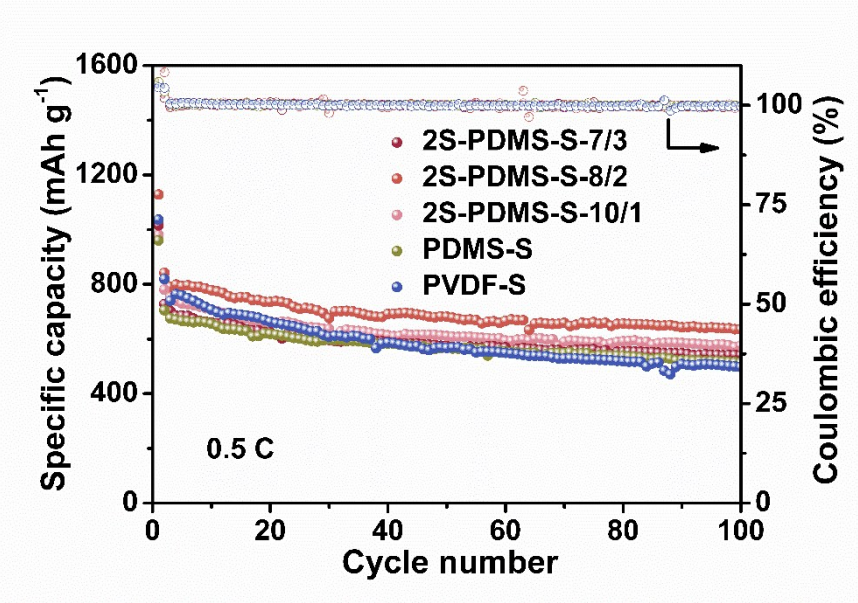

Fig. S18. Cycling performance of sulfur electrodes with different polymer binders at 0.5 C.

The introduction of a certain content of 2S compound in 2S-PDMS polymer can effectively enhance the specific capacity. However, the Li−S batteries using 2S-PDMS-7/3 binder (H_2N-PDMS-NH_2 to 2S molar ratio of 7:3) also show inferior cycling properties. It was attributed to poor self-healing characteristic (Fig. S21) and bigger charge-transfer resistance of 60 Ω (Fig. S19). In addition, 2S-PDMS-8/2 show a sub-optimal performance when used as binders in Li−S batteries, benefited by its abundant dynamic disulfide bonds which can accelerate the conversion of polysulfides and enhance the capacity of batteies, but the inferior self-healing behavior resitrict the further enhancement of capacity. For 2S-PDMS-10/1, insufficient disulfide bonds were introduced in molecules, resulting in limited improvement of capacity despite its superior self-healing charactersitic. Binders with stronger self-healing characterisitic can better supperess the loss of active materials resulted from volume variation of electrodes during charge/discharge, and hence can improve the capacity during cycling.

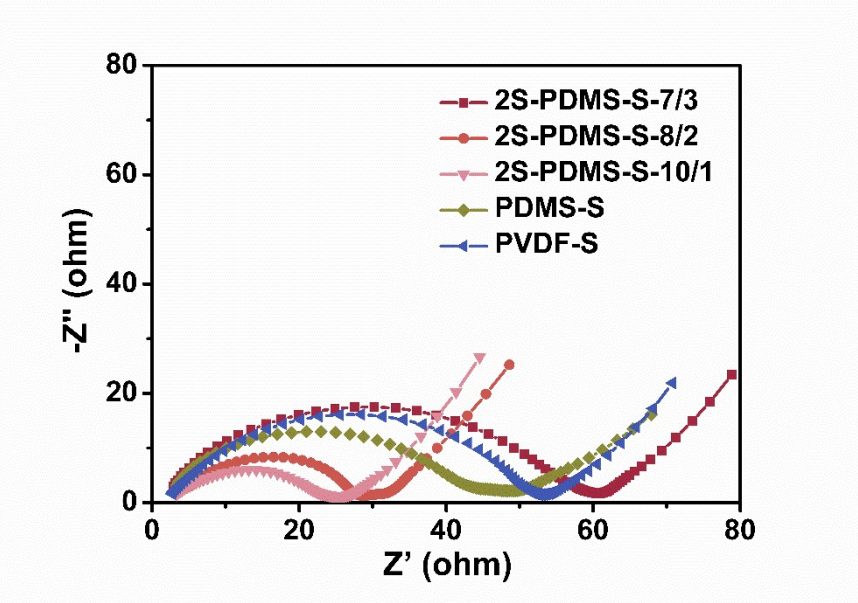

Fig. S19. EIS curves of sulfur electrode with different polymer binders.

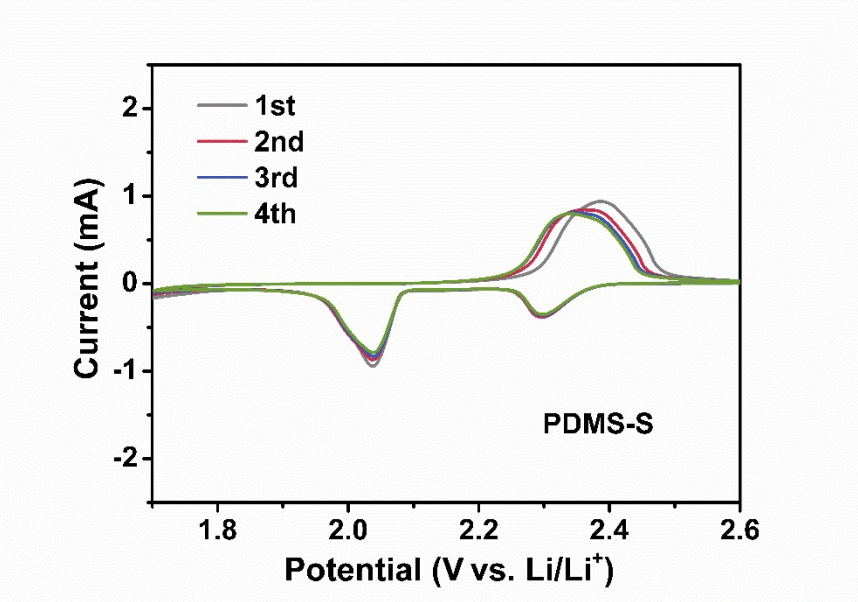

Fig. S20. CV curves of the first four scan for PDMS-S electrode at a scan rate of 0.1 mVs^{-1}.

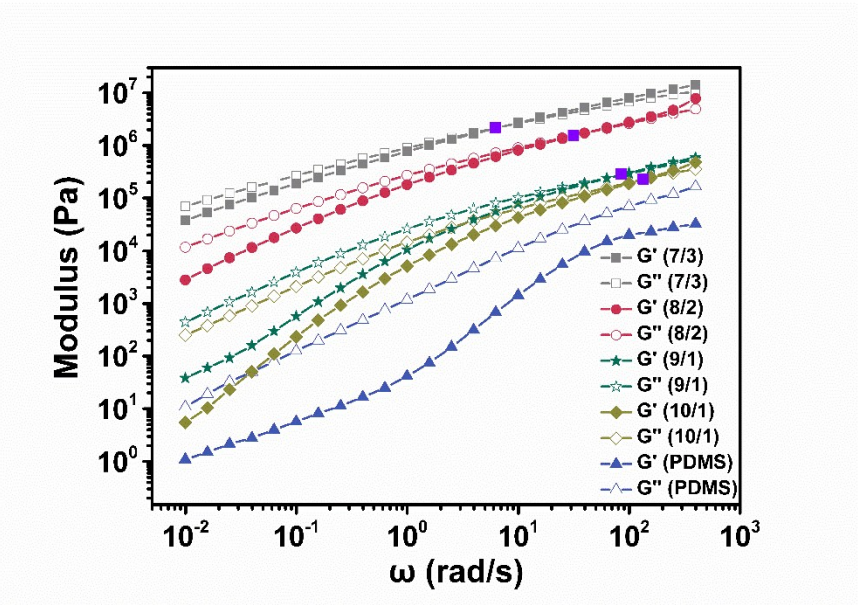

Fig. S21. Frequency sweep measurement of 2S-PDMS polymer using different mixing molar ratio of H_2N-PDMS-NH_2 and 2S. The purple squares represent the intersection of G' and G".

The rheological data at 25 °C showed that G' was lower than G" at low frequency and higher at high frequency. The characteristic relaxation time of the polymer was calculated from the frequency of the intersection point (purple squares) in the curves. The characteristic relaxation time became longer with the increase of 2S content, which indicated ever worse self-healing ability.

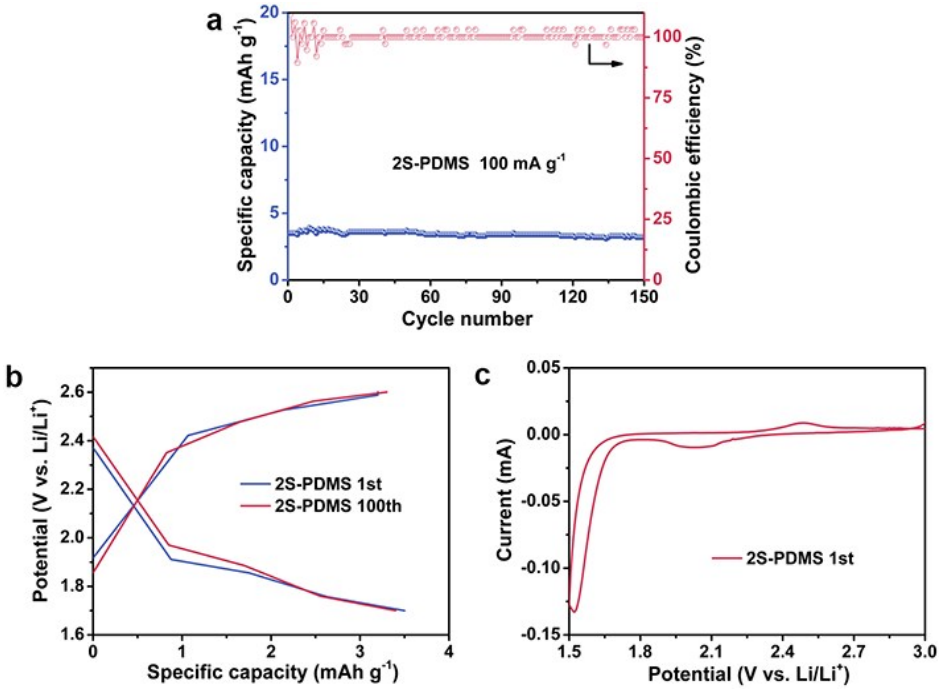

Fig. S22. (a) Cycling performance of 2S-PDMS/AB electrode at a current density of 100 mA g^{-1} and the (b) corresponding galvanostatic charge-discharge profiles. (c) CV curves of the 2S-PDMS/AB electrode at first scan.

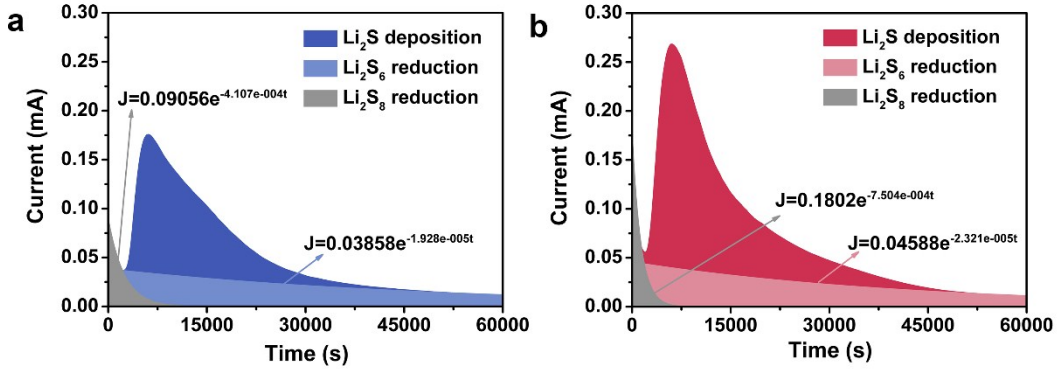

Fig. S23. Potentiostatic discharge curves of a Li_2S_8/tetraglyme solution at 2.04 V on (a) PVDF/CP and (b) 2S-PDMS/CP interfaces after galvanostatically discharged at 0.112 mA to 2.05 V, respectively.

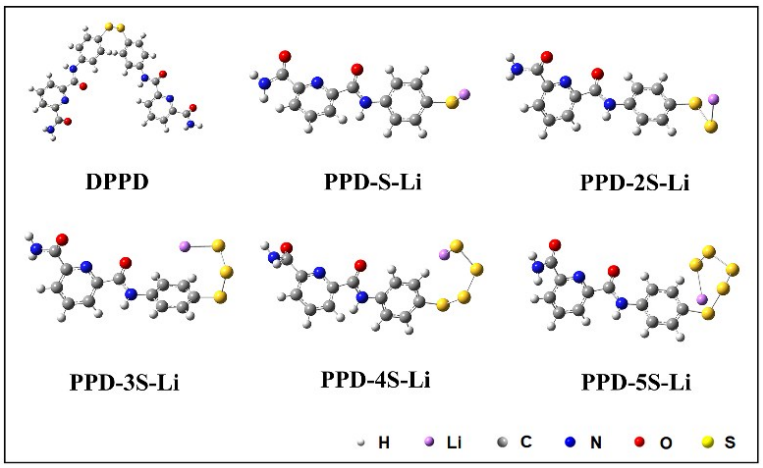

Fig. S24. Fully optimized structures of the reacting products obtained between polysulfides (Li_2S_n) and part of 2S-PDMS molecules. The white, magenta, gray, blue, red, and yellow colors represent hydrogen, lithium, carbon, nitrogen, oxygen, and sulfur atoms, respectively.

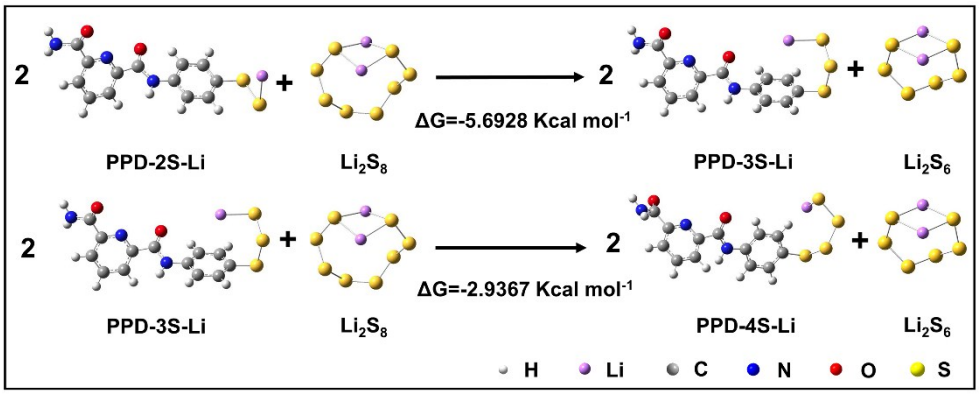

Fig. S25. Density functional theory calculations. Gibbs free energy of polysulfides conversion reaction acquired from quantum chemistry calculation.

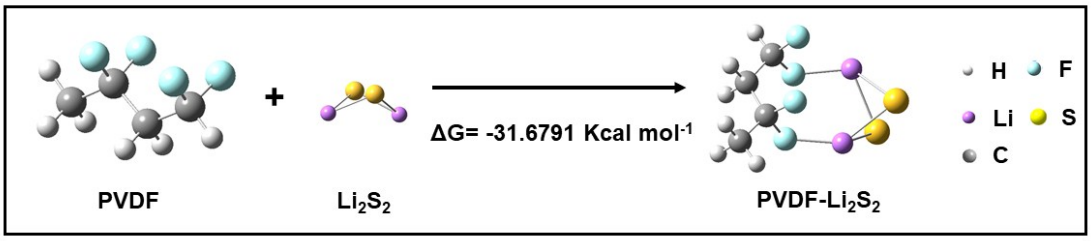

Fig. S26. The calculation of Gibbs free energy of the reaction between PVDF model molecule and Li_2S_2.

According to the literatures,[14] PVDF can interact with Li_2S_2 through Li-F bond and form an adsorption complex rather than break chemical bond. Single point energy calculations of PVDF molecular models[15] and reacting product are calculated as -555.2353 eV and -1366.5385 eV, respectively. Based on these data, the Gibbs free energy of the reaction between PVDF model molecules and Li_2S_2 is -31.6791 Kcal mol^{-1}, indicating that PVDF has the ability to adsorb Li_2S_2.

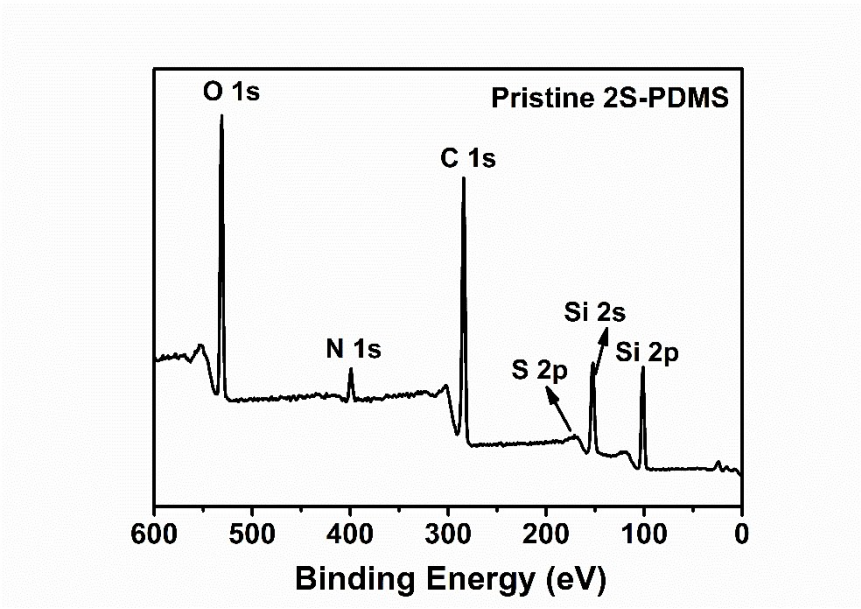

Fig. S27. XPS spectrum of the 2S-PDMS binder.

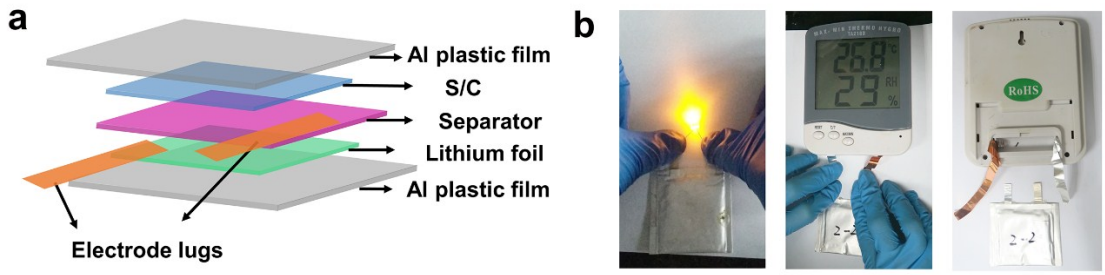

Fig. S28. (a) Schematic illustration of soft-packed Li−S batteries assembled using 2S-PDMS-S electrode. (b) Optical images of 2S-PDMS-S based soft-packed batteries lighting up an LED lamp and electronic hygrothermograph.

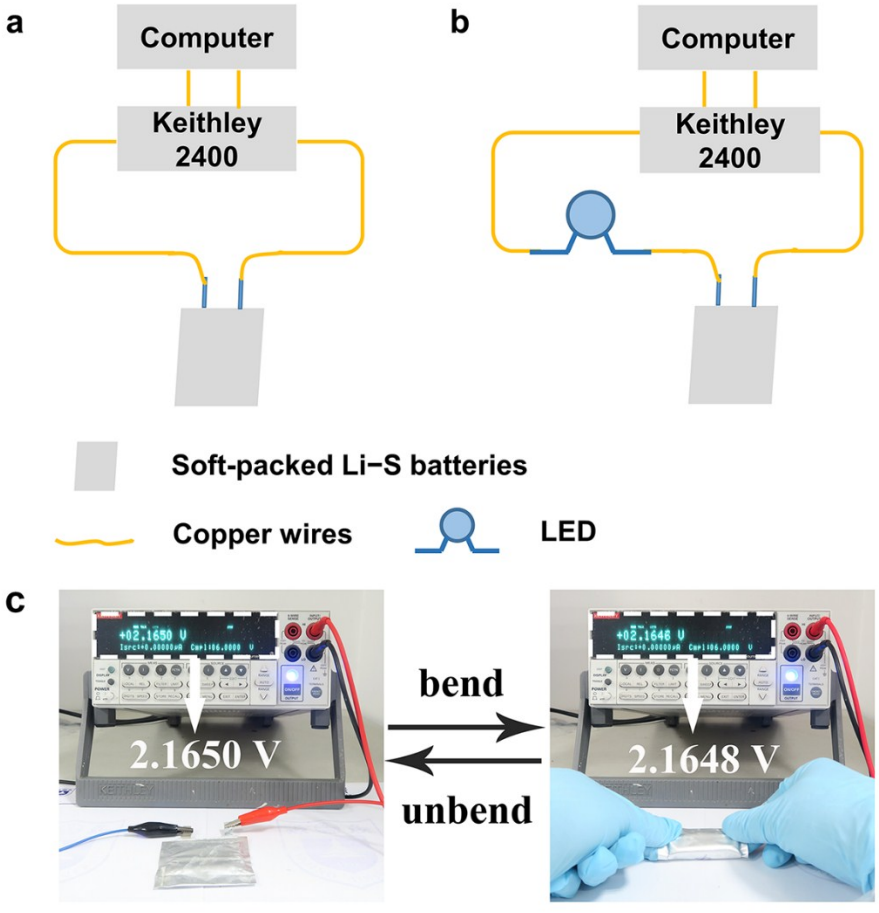

Fig. S29. Circuit diagrams of current (a) and voltage (b) monitored by a Keithley 2400 instrument. (c) 2S-PDMS-S based soft-packed Li−S batteries were connected to keithley 2400 in order to monitor voltage changes in the circuit before and after the bending test.

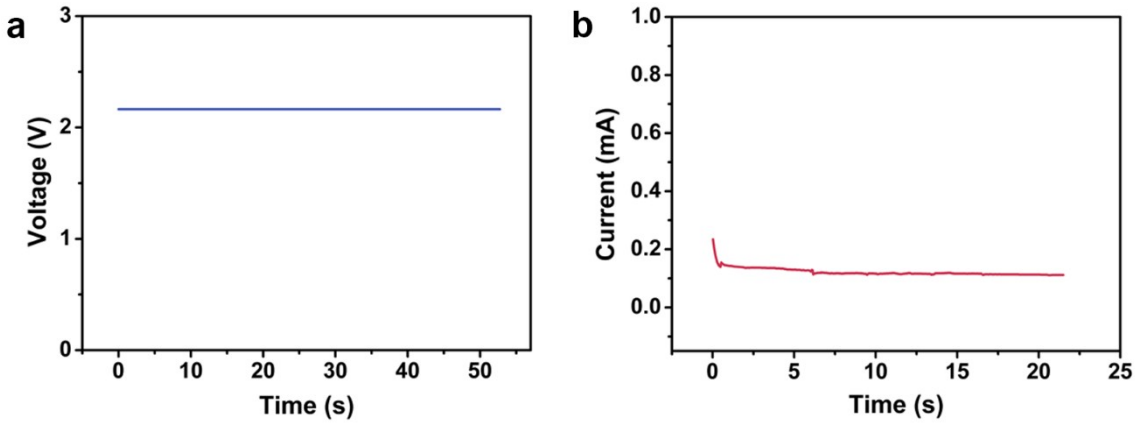

Fig. S30. The voltage curves (a) and current curves (b) under continuous bending-unbending operations in the circuit.

Table S1. Single point energy calculations of polysulfides and reacting products obtained between polysulfides (Li_2S_n) and part of 2S-PDMS molecules.

Polysulfides	Li_2S	Li_2S_2	Li_2S_4	Li_2S_6	Li_2S_8	DPPD
G (eV)	-413.2011	-811.2527	-1607.3368	-2403.4064	-3199.4650	-2425.3396
Products	PPD-S-Li	PPD-2S-Li	PPD-3S-Li	PPD-4S-Li	PPD-5S-Li	
G (eV)	-1220.2644	-1618.2978	-2016.3316	-2414.3632	-2812.3898	

Table S2. DFT calculations of the variation of Gibbs free energy (eV) for the various conversion reactions of polysulfides (Li_2S, Li_2S_2, Li_2S_4, Li_2S_6 and Li_2S_8) with different species in 2S-PDMS molecules.

Conversion reactions	**Δ*G* (eV)**
1.DPPD/Li_2S_n	
(1.1) DPPD + Li_2S_2 →2PPD-2S-Li	-0.0032
(1.2) DPPD + Li_2S_4 →2PPD-3S-Li	0.0132
(1.3) DPPD + Li_2S_6 →2PPD-4S-Li	0.0195
(1.4) DPPD + Li_2S_8 →2PPD-5S-Li	0.0249
2.PPD-S-Li/Li_2S_n	
(2.1) PPD-S-Li + Li_2S_2 →PPD-2S-Li + Li_2S	0.0183
(2.2) 2PPD-S-Li + Li_2S_4 →2PPD-2S-Li + Li_2S_2	0.0173
(2.3) 2PPD-S-Li + Li_2S_6 →2PPD-2S-Li + Li_2S_4	0.0029
(2.4) 2PPD-S-Li + Li_2S_8 →2PPD-2S-Li + Li_2S_6	-0.0082
3. PPD-2S-Li/Li_2S_n	
(3.1) PPD-2S-Li + Li_2S_2 →PPD-3S-Li + Li_2S	0.0178
(3.2) 2PPD-2S-Li + Li_2S_4 →2PPD-3S-Li + Li_2S_2	0.0164
(3.3) 2PPD-2S-Li + Li_2S_6 →2PPD-3S-Li + Li_2S_4	0.0019
(3.4) 2PPD-2S-Li + Li_2S_8 →2PPD-3S-Li + Li_2S_6	-0.0091
4. PPD-3S-Li/Li_2S_n	
(4.1) PPD-3S-Li + Li_2S_2 →PPD-4S-Li + Li_2S	0.0200
(4.2) 2PPD-3S-Li + Li_2S_4 →2PPD-4S-Li + Li_2S_2	0.0207
(4.3) 2PPD-3S-Li + Li_2S_6 →2PPD-4S-Li + Li_2S_4	0.0063
(4.4) 2PPD-3S-Li + Li_2S_8 →2PPD-4S-Li + Li_2S_6	-0.0047
5. PPD-4S-Li/Li_2S_n	
(5.1) PPD-4S-Li + Li_2S_2 →PPD-5S-Li + Li_2S	0.0250
(5.2) 2PPD-4S-Li + Li_2S_4 →2PPD-5S-Li + Li_2S_2	0.0308
(5.3) 2PPD-4S-Li + Li_2S_6 →2PPD-5S-Li + Li_2S_4	0.0164
(5.4) 2PPD-4S-Li + Li_2S_8 →2PPD-5S-Li + Li_2S_6	0.0054

References

1. P. J. Stephens, F. J. Devlin, C. F. Chabalowski and M. J. Frisch, *J. Phys. Chem.,* 1994, **98**, 11623.
2. R. Ditchfield, W. J. Hehre and J. A. Pople, *J. Chem. Phys.,* 1971, **54**, 724.
3. W. J. Hehre, R. Ditchfield and J. A. Pople, *J. Chem. Phys.,* 1972, **56**, 2257.
4. P. C. Hariharan and J. A. Pople, *Theor. Chim. Acta.,* 1973, **28**, 213.
5. M. M. Francl, W. J. Pietro, W. J. Hehre, J. S. Binkley, M. S. Gordon, D. J. DeFrees and J. A. Pople, *J. Chem. Phys.,* 1982, **77**, 3654.
6. S. Grimme, *J. Chem. Phys.,* 2006, **124**, 034108.
7. F. Weigend and R. Ahlrichs, *Phys. Chem. Chem. Phys.,* 2005, **7**, 3297.
8. J. L. Pascual-ahuir, E. Silla, and I. Tuñon, *J. Comput. Chem.,* 1994, **15**, 1127.
9. S. Miertuš, E. Scrocco, and J. Tomasi, *Chem. Phys.,* 1981, **55**, 117.
10. B. Mennucci, *Wiley Interdiscip. Rev. Comput. Mol. Sci.,* 2012, **2**, 386.
11. E. Cancès, B. Mennucci and J. Tomasi, *J. Chem. Phys.,* 1997, **107**, 3032.
12. B. Mennucci, E. Cancès and J. Tomasi, *J. Phys. Chem. B,* 1997, **101**, 10506.
13. M. J. Frisch, G. W. Trucks, H. B. Schlegel, G. E.Scuseria, M. A. Robb, J. R. Cheeseman, G. Scalmani, V. Barone, B. Mennucci, G. A. Petersson, H. Nakatsuji, M. Caricato, X. Li, H. P. Hratchian, A. F. Izmaylov, J. Bloino, G. Zheng, J. L. Sonnenberg, M. Hada, M. Ehara, K. Toyota, R. Fukuda, J. Hasegawa, M. Ishida, T. Nakajima, Y. Honda, O. Kitao, H. Nakai, T. Vreven, J. A. Montgomery, Jr., J. E. Peralta, F. Ogliaro, M. Bearpark, J. J. Heyd, E. Brothers, K. N. Kudin, V. N. Staroverov, R. Kobayashi, J. Normand, K. Raghavachari, A. Rendell, J. C. Burant, S. S. Iyengar, J. Tomasi, M. Cossi, N. Rega, J. M. Millam, M. Klene, J. E. Knox, J. B. Cross, V. Bakken, C. Adamo, J. Jaramillo, R. Gomperts, R. E. Stratmann, O. Yazyev, A. J. Austin, R. Cammi, C. Pomelli, J. W. Ochterski, R. L. Martin, K. Morokuma, V. G. Zakrzewski, G. A. Voth, P. Salvador, J. J. Dannenberg, S. Dapprich, A. D. Daniels, Ö. Farkas, J. B. Foresman, J. V. Ortiz, J. Cioslowski and D. J. Fox, Gaussian, Inc.,Wallingford CT, *Gaussian* 09, Revision B.01, 2010.
14. G. Zhou, K. Liu, Y. Fan, M. Yuan, B. Liu, W. Liu, F. Shi, Y. Liu, W. Chen, J. Lopez, D. Zhuo, J. Zhao, Y. Tsao, X. Huang, Q. Zhang and Y. Cui, *ACS Cent. Sci.*, 2018, **4**, 260.
15. J. B. Liao, Z. Liu, X. D. Liu and Z. B. Ye. *J. Phys. Chem. C*, 2018, **122**, 25917.